Stem Cell Reports
Article

ISSCR

OPEN ACCESS

Lineage Tracing and Cell Potential of Postnatal Single Progenitor Cells *In Vivo*

María Figueres-Oñate,[1,2] Mario Sánchez-Villalón,[1] Rebeca Sánchez-González,[1] and Laura López-Mascaraque[1,*]

[1]Instituto Cajal-CSIC, Madrid, Spain
[2]Present address: Max Planck Research Unit for Neurogenetics, Frankfurt am Main, Germany
*Correspondence: mascaraque@cajal.csic.es
https://doi.org/10.1016/j.stemcr.2019.08.010

SUMMARY

Understanding the contribution of adult neural progenitor cells (NPCs) and their lineage potential is a great challenge in neuroscience. To reveal progenitor diversity and cell-lineage relationships of postnatal NPCs in the subventricular zone (SVZ), we performed *in vivo* lineage-tracing genetic analysis using the *UbC-StarTrack*. We determined the progeny of single SVZ-NPCs, the number of cells per clone, the dispersion of sibling cells, and the cell types within clones. Long-term analysis revealed that both the cell-dispersion pattern and number of cells comprising clones varied depending on the glial/neuronal nature of sibling cells. Sibling-olfactory interneurons were primarily located within the same layer, while sibling-glial cells populated SVZ-adjacent areas. Sibling astrocytes and interneurons did not form big clones, whereas oligodendroglial-lineage clones comprised the largest clones originated in adult brains. These results demonstrate the existence of SVZ postnatal bipotential progenitors that give rise to clones widely dispersed across the olfactory bulb and SVZ-adjacent areas.

INTRODUCTION

Adult mammalian brains contain a major neurogenic niche in the subventricular zone (aSVZ) lining the walls of the lateral ventricles. Neural progenitor cells (NPCs) in this region generate cells that progress through distinct developmental stages to generate mature functional cells (Kriegstein and Alvarez-Buylla, 2009). The glial nature of adult NPCs (aNPCs) is evident, as embryonic radial glial cells directly transform into progenitors that persist within the aSVZ (Merkle et al., 2004). Moreover, some aNPCs derive from embryonic precursors located in the same region (Fuentealba et al., 2015), although a mixture of NPCs from different areas coexist at perinatal stages in the SVZ (Willaime-Morawek et al., 2006; Young et al., 2007).

Astrocyte-like stem cells from the aSVZ divide slowly and give rise to neuroblasts (NBs) via transit-amplifying progenitors (TAPs) (Alvarez-Buylla and Garcia-Verdugo, 2002). These SVZ-derived NBs travel tangentially via the rostral migratory stream (RMS) to the olfactory bulb (OB), where they switch to radial migration to differentiate into granular/periglomerular interneurons (Doetsch and Alvarez-Buylla, 1996). The SVZ neurogenic niche includes different microdomains, which are linked to the generation of specific OB interneuron subtypes (Fiorelli et al., 2015; Merkle et al., 2014). Thus, the heterogeneity of SVZ-NPCs underlies the different OB interneurons that arise due to a combination of transcription factors and morphogens (Ihrie et al., 2011). Furthermore, NPCs proliferate and give rise to multilineage precursors both *in vivo* (Ganat et al., 2006; Levison and Goldman, 1997) and *in vitro* (Laywell et al., 2000; Ortega et al., 2013), although *in vivo* generation of different lineages from a single postnatal NPC (pNPC) remains unresolved (Dimou and Götz, 2014; Obernier and Alvarez-Buylla, 2019).

Single-cell transcriptomic analyses revealed new data on cell heterogeneity. These data show the variability of gene expression within the neurogenic niche in active or quiescent NPCs resulting from either physiological conditions or brain injury (Beckervordersandforth et al., 2010; Codega et al., 2014; Llorens-Bobadilla et al., 2015). Such results are primarily analyzed by considering the whole population of ventricular NPCs, which are isolated by the co-expression of different markers. However, NPC populations with similar morphological and molecular identities could exhibit variable self-renewal and differentiation capacities.

Cell diversity is more likely based on single progenitor potential rather than NPC pools, and analysis of this requires the use of cell lineage tracking at single-cell level (Calzolari et al., 2015). Lineage transitions between NPCs and their derivatives occur via gradual maturation, mostly when there is co-expression of the same marker by different cell types. Therefore, no single molecular marker can unambiguously define an individual cell population. Clonal analysis and lineage tracing have thus become crucial for clear identification of lineage progression (Bribián et al., 2016; Ma et al., 2018).

To improve lineage progression identification, we used the StarTrack methodology to trace both the clonal fate of astrocytes from single progenitors (García-Marqués and López-Mascaraque, 2013) and the whole lineage of single cells (Figueres-Oñate et al., 2015, 2016). Here, using

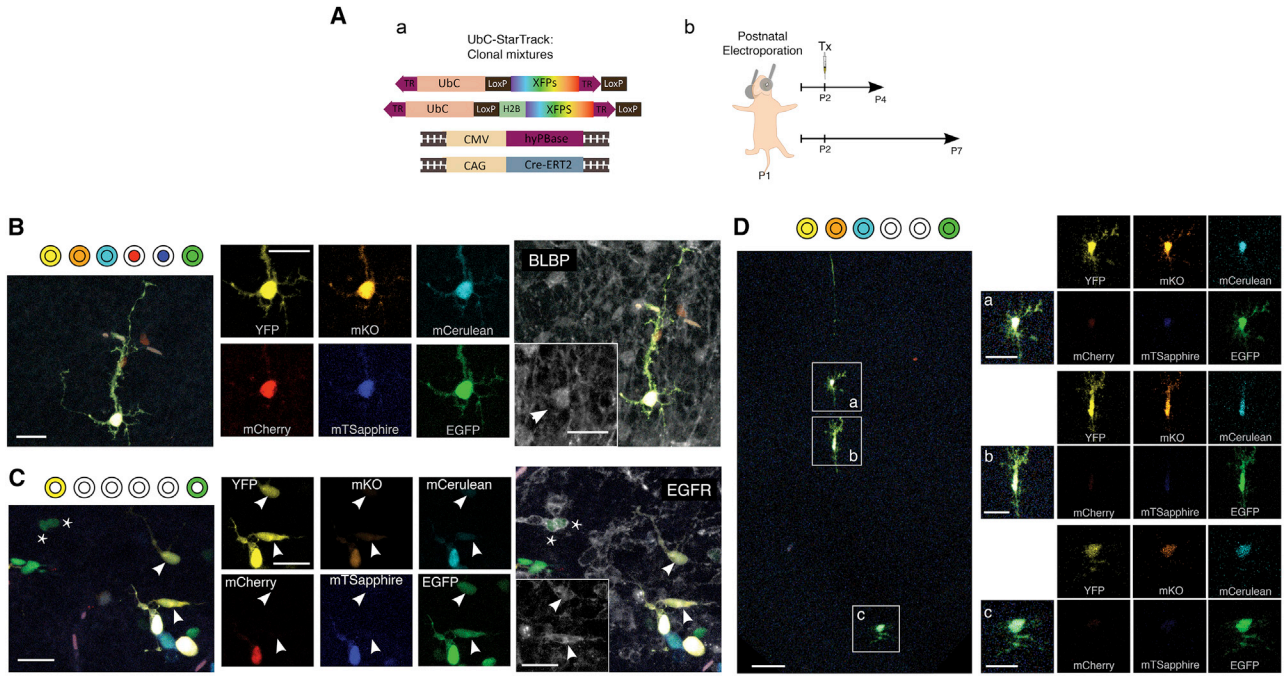

Figure 1. Early Cell Progeny of Postnatal NPCs

(A) (a) *UbC-StarTrack* clonal mixture includes 12 ubiquitous plasmids expressing six different fluorescent reporter proteins (XFPs) either in cytoplasm or in the nucleus (H2B). Co-electroporation with hyperactive *PiggyBac* transposase (hyPBase) and *Cre*-recombinase (*Cre*-ERT2) is required. (b) Postnatal electroporation was performed at P1. Tamoxifen administration 1 day after electroporation activated *Cre*-recombinase and eliminated non-integrated constructs. Brains were analyzed at 3 days (P4) and 7 days (P7) after electroporation.

(B) *UbC-StarTrack*-labeled NPCs express BLBP 3 days after electroporation. Scale bars, 25 μm.

(C) EGFR labels active NPCs as well as TAPs. Two clones containing pairs of sibling cells (arrowheads and stars) are shown 3 days after electroporation. Scale bars, 25 μm.

(D) Sibling astrocytes dispersed through the cortical layers 6 days after electroporation (P7). Labeled cells scattered into the cortex and other ventricular adjacent areas, displaying differentiated morphologies. The color codes are detailed in (a) to (c). Scale bars, 50 μm (D) and 25 μm (Da, Db, Dc).

UbC-StarTrack, we performed detailed *in vivo* analysis of the lineage progression of single targeted perinatal NPCs. Our aim was to gain further insight into the heterogeneity of the neural cell types that are generated by pNPCs. Additionally, NPC lineage tracing may provide further information regarding the specific characteristics of clonally related cells derived from the same NPC.

RESULTS

Short-Term Clonal Cell Progeny from Postnatal NPCs from the SVZ

Progenitors lining the lateral ventricles of postnatal day 1 (P1) mice were tagged using the *UbC-StarTrack* (Figure 1A) to provide specific and unique color coding of single pNPCs and their progeny. *UbC-StarTrack* is a combination of six different fluorescent reporter proteins expressed in the cytoplasm and/or nucleus (Figueres-Oñate et al., 2016). The system requires the co-electroporation of two additional constructs: the hyperactive transposase of the *PiggyBac* system (hyPBase), and a tamoxifen-inducible *Cre*-recombinase (*Cre*-ERT2) that inhibits non-integrated constructs to achieve stable and heritable cell labeling (Figure 1Aa).

The clonal mixture was injected into the ventricles of P1 mice, then electroporated into cells lining the dorsolateral SVZ. Tamoxifen was administered 24 h after electroporation to eliminate non-integrated constructs. Brains were analyzed at either P4 or P7 to assess the clonal expansion of the cells targeted with *UbC-StarTrack* (Figure 1Ab). At P4, the labeled cells were primarily located in the region adjacent to the dorsolateral ventricular area, revealing reduced dispersion a few days after targeting. Sibling cells were identified by their coincident color codes, and were considered to be clonally related cells. NPCs that were positive for brain lipid-binding protein (BLBP) were located near the ventricular surface at P4 (Figure 1B). Active NPCs are known to upregulate molecular markers such as

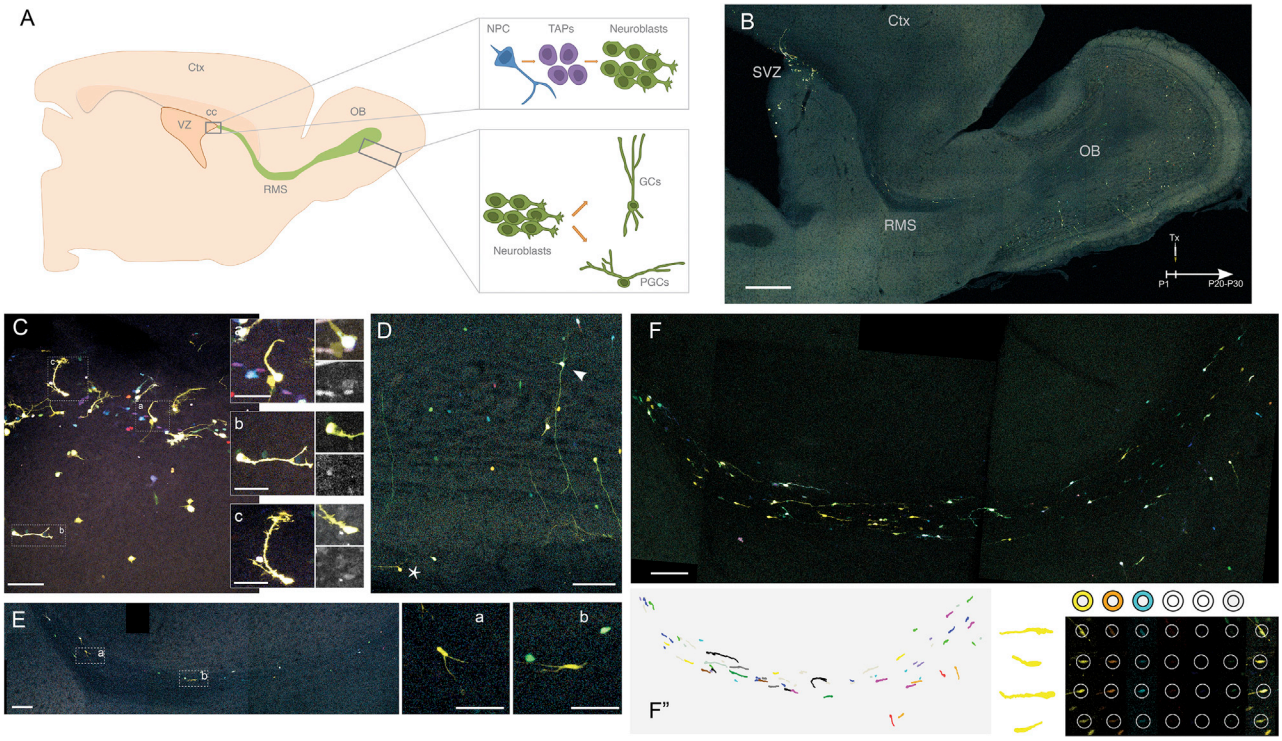

Figure 2. Short-Term Clonal Analysis of Postnatal NPCs

(A) Scheme of a sagittal brain section of adult mice. NPCs give rise to TAPs that generate NBs in SVZ. These NBs migrate to the OB via RMS to differentiate into GCs or PGCs in the OB.

(B) *UbC-StarTrack*-labeled cells 20–30 days after electroporation. Differentiated cells located along the SVZ-RMS-OB pathway. Sagittal section.

(C) Targeting cells in SVZ exhibits different morphologies according to the maturation stages, from more immature cells (a) to more branched shapes (c). Some cells display intermediate morphologies as bipolar cells (b). All cell morphologies are co-labeled with Sox2 antibody.

(D) Different localization of labeled cells in the OB. The arrowhead shows a mature GC, and the star identifies a PGC.

(E) Sagittal view of the RMS showing sibling neuroblast migrating though RMS (a and b).

(F) The dispersion pattern of sibling neuroblasts along the RMS, 20 dpe, are sparsely distributed throughout the migratory pathway. (F″) Image rendering from (F). Sibling cells labeled with the same fluorescent colors according to their color codes. An example of the true expression of fluorophores is shown.

Scale bars, 500 μm (B), 100 μm (C–F), and 50 μm (Ca, Cb, Cc, Ea, Eb). NPC, neural progenitor cells; TAPs, transit-amplifying progenitor cells; NBs, neuroblasts; GCs, granular cells; PGCs, periglomerular cells; SVZ, subventricular zone; RMS, rostral migratory stream; OB, olfactory bulb.

EGFR, and this continues to be expressed within the TAP population.

Interestingly, short-term analysis revealed pairs of sibling cells co-labeled with the EGFR marker, near the electroporated area (arrowheads and stars in Figure 1C). Thus, some NPCs had already divided 3 days after electroporation (P4), while others did not divide, as evidenced by the presence of single NPCs that were positive for BLBP (Figure 1B). At P7, the labeled cells reflected a wide dispersion pattern, displaying the mature features of glial cells (Figure 1D). Figures 1Da–1Dc display the migration of clusters of differentiating sibling astrocytes through the cortical layers.

Clonal Cell Pattern of Interneurons in the Adult Olfactory Bulb Generated from Postnatal NPCs

Postnatal progenitors produce TAPs that primarily generate NBs, which migrate along the RMS until they radially migrate to the OB to become granular or periglomerular cells (Figure 2A). To assess the time course of sibling cell progression along the SVZ-RMS-OB pathway, we analyzed the *UbC-StarTrack*-labeled cells targeted at P1 at young adult stages (P20–P30). At P30, labeled cells were identified along the entire pathway from the SVZ to the OB (Figure 2B). NPCs targeted at P1 displayed different features (Figure 2C), including NPC-like cells with an immature morphology (Figure 2Ca), bipolar cells at intermediate

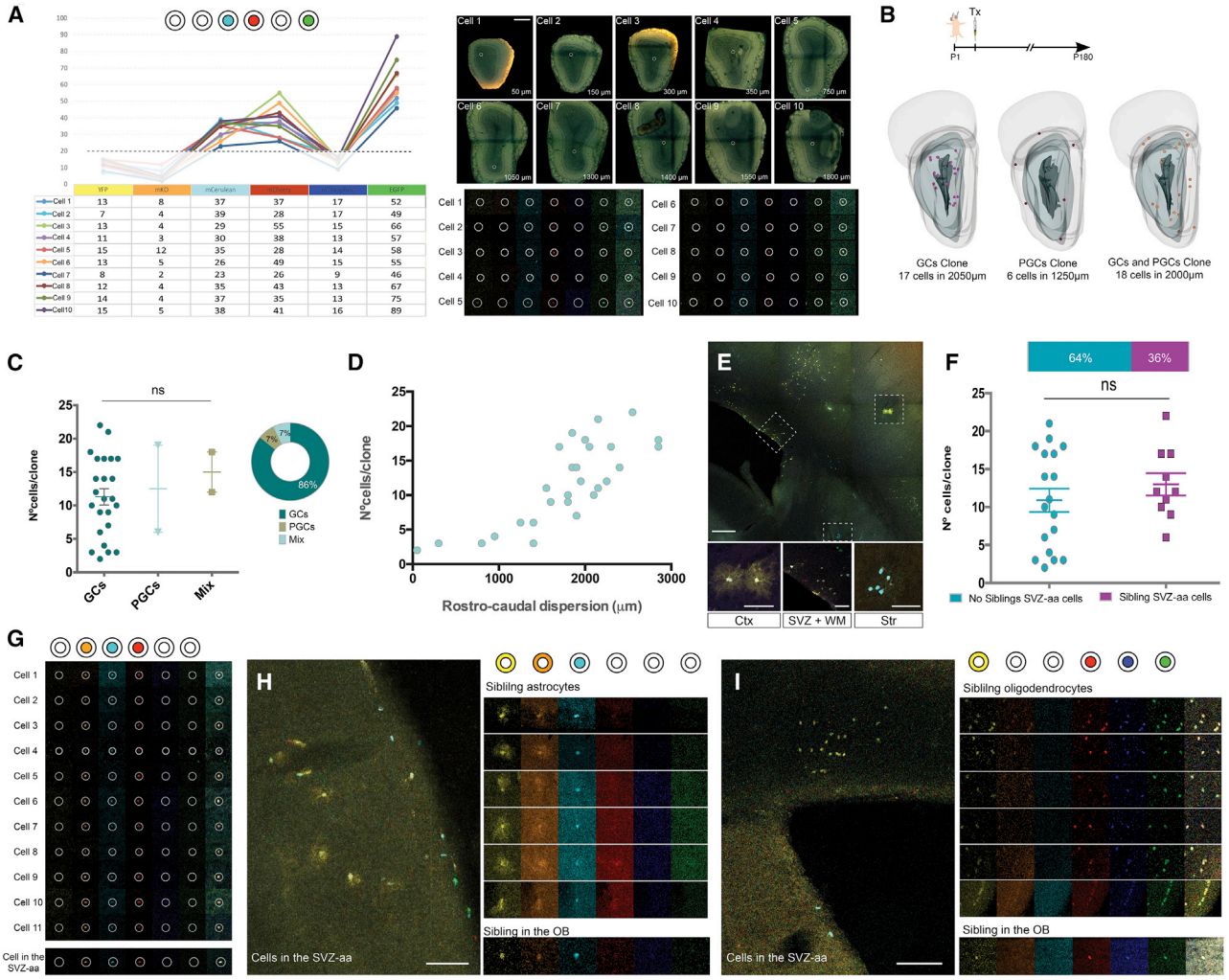

Figure 3. Clonal Pattern of Adult OB Interneurons at P180

(A) Graphical distribution of the fluorescent intensity in each channel of cells forming a clone. Further identification of nuclear and cytoplasmic labeling lead to the final color code. The clone formed by ten sibling interneurons was distributed across 1,800 µm throughout the OB rostrocaudal axis. Scale bar, 500 µm for all OBs. Specific color code is shown in the six different fluorescent channels for each sibling cell.

(B) Scheme of postnatal electroporation at P1 with tamoxifen administration 1 day after surgery to remove the episomal copies of UbC constructs. Tissues were analyzed at P180. Representative 3D clonal distribution patterns (n = 28) classified GCs, PGCs, and mix clones that included sibling cells of both types.

(C) No significant differences in the average clonal size between GCs (11.29 ± 1.21 cells), PGCs (12.50 ± 6.5 cells), or mix clones (15 ± 3 cells). The bulk of the analyzed clones consisted of sibling interneurons that belong to granule cells (GCs: 85.72%) and periglomerular cells (PGCs: 7.14%), and a mix of clones was located in both layers (7.14%).

(D) Clonal size increases according to the cell dispersion along the rostrocaudal OB axis.

(E) Top: labeled cells in the SVZ-aa coronal section. Scale bar, 250 µm. Bottom: detail of targeted cells in the cerebral cortex (Ctx), subventricular zone (SVZ), white matter (WM), and striatum (Str). Scale bars, 50 µm.

(F) At adult ages, 64% of clones were restricted to the OB (18 clones), while 36% of the OB clones had siblings in the SVZ-aa (10 clones). There was no significant difference between the size of OB interneuronal clones with or without siblings in the SVZ-aa.

(G) Clone of olfactory bulb interneurons formed by 11 cells displaying sibling cells in the SVZ-aa.

(H) Representative astroglial clone formed by six cells in the SVZ-aa (striatum) with sibling cells in the OB. Clonally related cells present the same fluorophore expression and location. Scale bar, 100 µm.

(legend continued on next page)

maturation stages (Figure 2Cb), and more branched morphologies (Figure 2Cc). NPCs were identified by the expression of the Sox2 antibody (Figures 2Ca–2Cc). In addition, interneurons with mature characteristics were located in the OB, in both the granular (GcL; arrowhead in Figure 2D) and glomerular layers (GL; star in Figure 2D). Sagittal sections (Figure 2E) showed clusters of immature cells migrating to the OB through the RMS, including some sibling NBs (Figures 2Ea and 2Eb). Sibling NBs appeared in clusters of 2–3 cells that were widespread along the RMS axis (Figure 2F and rendering of sibling cells in Figure 2F″). Together, these data reveal the clonal dispersion pattern of the cell progeny arising from pNPCs in young adults.

Long-term cell-dispersion analyses at 6 months post electroporation (P180) allowed us to uncover the clonal dispersion map of labeled OB interneurons. A total of 4,977 *UbC-StarTrack*-labeled cells were analyzed in four mice scattered across an average region of 2,713 ± 274 μm within the OB rostrocaudal axes. Because there was broad rostrocaudal dispersion of the sibling OB interneurons, the selected color codes for clonally related cells were taken from the less frequent combinations (Figueres-Oñate et al., 2016). Here, the number of analyzed combinations was increased by one order of magnitude (from 6,690 to 101,696 cells). However, the most frequent combinations of fluorophores that occurred in both studies were nearly identical (Table S1).

We employed a custom ImageJ macro to determine the clonal color codes. After the fluorescence intensity was measured for each fluorescent protein in all of the cells that were detected, fluorophore cell localization (cytoplasm and/or nucleus) was used to define the final color codes. The corresponding coordinates of each sibling cell were identified, allowing for spatial reconstruction of the entire clone within the OB (Figure 3A). Sibling cells were distributed throughout the OB in three well-defined clonal patterns relative to layer location (n = 28; Figure 3B and Video S1). Clones were restricted to either the GcL (85.72%) or GL (7.14%), or were present in both layers (mixed clones, 7.14%; Figure 3C), displaying no significant variation in the number of sibling cells per clone (granular cells [GCs], 11.29 ± 1.21; periglomerular cells [PGCs], 12.50 ± 6.5; mix, 15 ± 3; Figure 3C). The ratio of GCs/PGCs in the mixed clones was 1:1 (Figure S1A), and their distribution appeared to be arbitrary along the rostrocaudal axis (Figure S1B). The neuronal OB clones exhibited different spatial distribution patterns along the rostrocaudal axis, with larger cell clones occupying broader domains (2,900 μm, Figure 3D).

As labeled cells were also identified in the targeted SVZ and adjacent areas (SVZ-aa), we considered whether OB clones could have sibling cells in those regions. For contexts under which cell identity was unclear, immunostaining was performed to assess the cell-type profile: glial fibrillary acidic protein (GFAP) to identify NPCs along the ventricular surface (Figure S2A); calretinin to characterize OB interneurons (Figure S2B); S100β to identify astrocytic cells (Figure S2C); and Olig2 to identify the oligodendroglial population located in the SVZ-aa (Figure S2D). Different numbers of labeled cells were spread in the SVZ, with an average scatter of 2,688 ± 769 μm along the rostrocaudal axis (Figure S3A). Most SVZ-aa cells were positioned close to the dorsal or lateral parts of the ventricles, although labeled cells with a sparse distribution were also found in adjacent striatal, subcortical white matter (WM), and cortical areas (Figure 3E). Interestingly, 64.29% of the cells had no siblings in the SVZ-aa. No significant clonal size differences were found between OB clones with (13 ± 1.4 cells/clone) or without (10.90 ± 1.5 cells/clone) SVZ-aa siblings (Figure 3F); neither were clonal size differences related to the location of sibling OB interneurons (Figures S3B and S3C). Moreover, of the 35.71% of clonally related OB interneurons that had sibling cells along the ventricular surface (Figure 3G), in some cases either sibling astrocytes (Figure 3H) or oligodendrocytes (Figure 3I) were identified. OB interneuron clones including sibling astrocytes and oligodendrocytes in the SVZ-aa indicate heterogeneity and bipotential capacity of the NPCs lining the dorsolateral area of the ventricular surface in postnatal stages.

Clonal Cell Patterns of Adult Glial Cells Arising from Postnatal NPCs

Next, we examined the fates and clonal relationships of the *UbC-StarTrack* labeled cells remaining in the SVZ-aa 6 months after electroporation. At P180, we analyzed a total of 5,907 labeled cells in the SVZ-aa from four different animals. Clones comprising astroglial or oligodendroglial lineages were located within the subcortical WM, striatum, and cerebral cortex. Clonally related astrocytes (n = 14), identified by equal fluorescent color codes (Figure 4A), were assembled in clusters of up to eight cells in adult brains. In addition, sibling astrocytes were positively correlated with clone size along the rostrocaudal axis of the SVZ-aa, with a maximum 250-μm intraclonal dispersion (Figure 4B). Astroglial clones were arranged in four different

(I) Clonally related cells, including oligodendroglial cells, in the SVZ-aa (white matter) and OB interneurons. The expression and location of the different fluorophores accurately defines sibling cells. Scale bar, 100 μm.

Values are presented as the mean ± SEM. Statistically significant differences across the groups are indicated as follows: ns, nonsignificant, $p > 0.05$. GCs, granular cells; PGCs, periglomerular cells; SVZ-aa, subventricular zone adjacent areas; IN, interneurons.

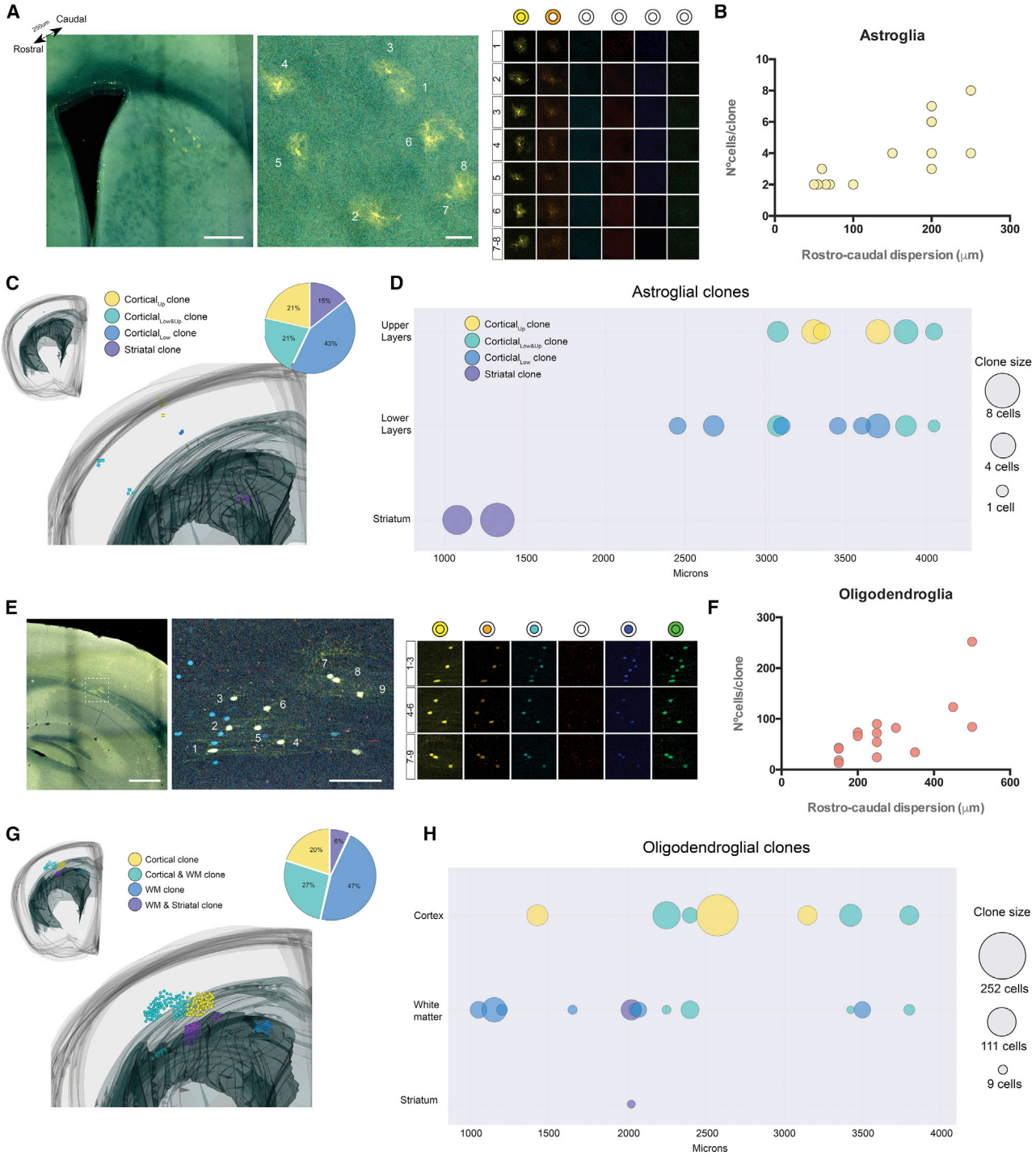

Figure 4. Clonal Pattern of Glial Lineages at P180

(A) Astroglial clone in the striatum formed by eight sibling cells identified by both labeling and cell location of the six fluorophores. Scale bars, 500 μm (left) and 50 μm (right).

(B) Larger astroglial clones occupy wider domains within the rostrocaudal axes, with a maximum of 250 μm of dispersion.

(C) 3D representation of sibling astroglial types located in the telencephalon after postnatal NPC targeting. Yellow: sibling astrocytes limited to the upper layers of the cerebral cortex (Cortical$_{up}$ clones, 21%); green: sibling astrocytes widespread into the lower and upper cortical layers (Cortical$_{low\&up}$ clones, 21%); blue: astroglial clones localized in the lower cortical layers (Cortical$_{low}$ clones, 43%); purple: sibling astrocytes restricted to the striatal region (Striatal clones, 15%).

(legend continued on next page)

distribution patterns and occupied either the striatal or cortical areas (Figure 4C and Video S2).

Within cortical areas, we distinguished three different clone locations: clones populating the upper cortical layers (from layers I to IV, named $Cortical_{up}$), clones colonizing the lower cortical layers (layers V and VI, named $Cortical_{low}$), and clones with sibling cells along the entire cortex (named $Cortical_{low\&up}$). Interestingly, $Cortical_{low\&up}$ clones had a cell ratio of 1:1.3 in populating lower and upper cortical areas, respectively (Figure S4A). Astroglial clones were also found in the striatum. Most of the astroglial clones were $Cortical_{low}$ (42.85%), followed by $Cortical_{up}$ (21.43%), with $Cortical_{low\&up}$ (21.43%), being the most infrequent clone type located in the striatum (14.28%; Figure 4C). To establish whether the location of astroglial clones was related to a preferential rostrocaudal distribution, we compiled all clones after normalizing rostral and caudal regions among different animals. Striatal clones tended to be found in more rostral positions, while $Cortical_{low\&up}$ and $Cortical_{up}$ clones were primarily located in caudal locations (Figure 4D). Analyses of clone size in relation to the SVZ-aa location showed that striatal clones (7 ± 1 cells/clone) tended to be bigger than lower cortical (2.5 ± 0.34 cells/clone) and upper cortical clones (3.33 ± 0.66; Figure S4B).

Oligodendroglial clones were located in domains within the SVZ-aa, including the striatum, subcortical WM, and cortex. Sibling cells, identified by the expression of identical color codes, were in close proximity to each other (Figure 4E). Regarding clone size, at P180, cells committed to oligodendroglial lineage formed the largest clones (from 13 to 252 cells, n = 15). The intraclonal cell dispersion reached 500 μm, suggestive of a positive correlation between clonal size and rostrocaudal dispersion (Figure 4F).

Regarding their location in the SVZ-aa, oligodendroglial clones were categorized as cortical clones, WM clones, clones including cortical and WM cells, and WM clones with some siblings in the striatum (Figure 4G and Video S3). The majority of oligodendroglial clones were located in the WM (46.67%), followed by Cortical&WM clones (26.66%) and cortical clones (20%). Less frequently identified clones populated the WM, with some cells seen to be invading the adjacent striatum (WM&Striatal clones, 6.67%) (Figure 4G). Sibling cells of Cortical&WM clones were distributed at a ratio of 1:3.2 throughout WM and cortical regions, respectively (Figure S4C). Oligodendroglial clones that were analyzed in all brains were normalized along the rostrocaudal axis to provide a complete view of the clone subtype, clone size, and rostrocaudal localization (Figure 4H). We observed no significant differences between clone size in relationship to SVZ-aa or rostrocaudal distribution (average: striatum + WM 73 cells/clone; WM 37.57 ± 9.72 cells/clone; WM + cortex 90.25 ± 11.23 cells/clone; cortex 124 ± 64.09 cells/clone) (Figure S4D).

Heterogeneity of the Postnatal NPC Pool: Specific Clonal Patterns Depend on Cell Lineage

The distinct lineages generated from pNPCs located in the dorsolateral SVZ displayed different clonal behaviors. With respect to the number of cells per clone, the oligodendroglial lineage produced the largest number of clones, with an average of 71.27 ± 15.10 cells/clone. Next were interneurons with an average of 11.64 ± 1.11 cells/clone, and the smallest clones were sibling astrocytes with an average of 3.93 ± 0.55 cells/clone (Figure 5A).

Interestingly, for all lineages, clone size and rostrocaudal dispersion were positively correlated (interneurons, r = 0.7936; astrocytes, r = 0.7868; oligodendrocytes, r = 0.7178), indicating a tendency for larger clones to populate broader domains (Figure 5B). The strength of this correlation was highly dependent on cell lineage. Even forming larger clones, glial lineages occupied smaller regions compared with interneurons. OB interneuronal clones, which are significantly smaller than oligodendroglial clones, tended to occupy a rostrocaudal distribution that was 5-fold microns greater than that of oligodendroglial clones.

Finally, to assess the cell potential of single pNPCs, we conducted an in-depth analysis of the distinct cell types included in clones with siblings located in both the OB and SVZ-aa or in either the OB or SVZ-aa (n = 49 clones) alone. These data showed that the most clones were purely

(D) General distribution of astroglial clones (n = 14) plotted according to their location along the rostrocaudal axes, clonal size, and layer distribution.

(E) Representative oligodendroglial clone in white matter (coronal section). Nine sibling oligodendrocytes identified by their color code are located in the white matter. Scale bars, 500 μm (left) and 50 μm (right).

(F) Rostrocaudal dispersion of oligodendroglial clones. Sibling cells occupy up to 500 μm in the rostrocaudal axis.

(G) 3D representation of oligodendroglial clone distribution within the telencephalon. Yellow: sibling oligodendroglial cells confined to the cortical layers (20%, Cortical clones); green: oligodendroglial clones located in both cortex and subcortical white matter (27%, Cortical&WM clones); blue: sibling oligodendrocytes limited to subcortical white matter (47%, WM clones); purple: sibling oligodendrocytes located in both white matter and striatum (6%, WM&Striatal clones).

(H) Representation of oligodendroglial clones (n = 15) plotted according to their location along the rostrocaudal axes, clonal size, and layer distribution.

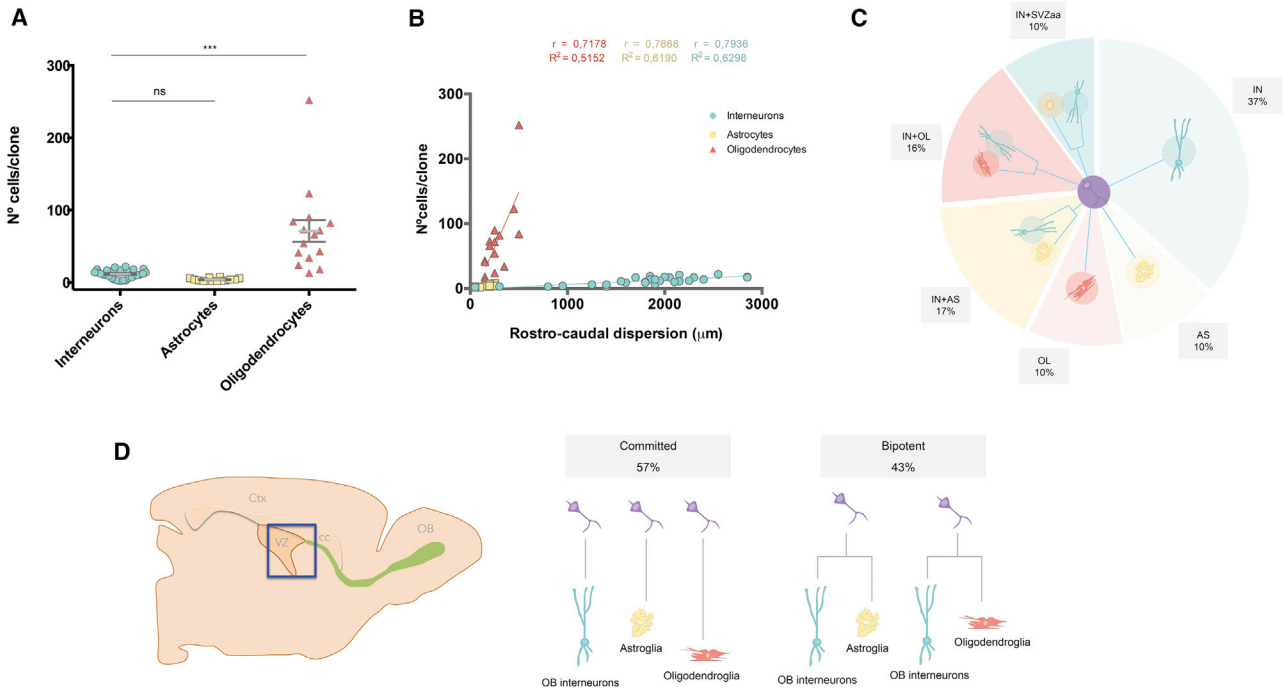

Figure 5. Clonal Relationships and Cell Potential of NPCs

(A) The number of sibling cells per clone significantly increased from interneuronal and astroglial to oligodendroglial clones.

(B) Correlation analysis showed positive correspondence between clonal size in terms of cell number and dispersion along the rostrocaudal axes in all cell lineages produced by pNPCs analyzed 6 months after targeting.

(C) Heterogeneity of postnatal NPCs. Thirty-seven percent of the OB interneurons (IN) did not present siblings in the SVZ-aa. Ten percent of astrocytes (AS) and 10% of oligodendrocytes (OL) arose from committed progenitor cells at P1. Sixteen percent of oligodendroglia (IN + OL) and 17% of astroglia (IN + AS) arose from a bipotent progenitor cell. Some cell identity in the SVZ-aa with OB could not be established and designated as IN + SVZ-aa clones (10%).

(D) Schematic diagram depicting the NPC potential after targeting the dorsolateral ventricular area at P1. NPCs give rise to glial cell lineages in addition to olfactory interneurons. Fifty-seven percent of clones were only formed by one lineage while 43% of the analyzed clones displayed gliogenic and neurogenic conformation.

Values are presented as the mean ± SEM. Statistically significant differences across the groups are indicated as follows: ns, nonsignificant, $p > 0.05$; ***$p \leq 0.001$.

neurogenic (IN, 37%), while only 20% clones were gliogenic (10% oligodendrogenic [OL] and 10% astrogenic [AS]). We thus concluded that these clones came from the committed NPCs, which were lining the ventricles at P1. On the other hand, 17% of the analyzed clones in our data were formed by both OB interneurons and sibling astrocytes (IN + AS), and 16% were formed by sibling interneurons and oligodendrocytes (IN + OL). Some OB clones had siblings in the SVZ-aa that could not be clearly identified based on morphology or immunohistochemistry because only a single fluorescent channel (far red) was available to perform immunostaining per section (named IN + SVZ-aa clones, 10%) (Figure 5C).

To summarize, pNPCs lining the dorsolateral SVZ produced distinct glial lineages that populated cortical, WM, and striatal areas, in addition to interneurons distributed throughout the OB, in either the GcL or GL. The lineage composition of the analyzed clones showed that 57% of the clones came from committed NPC cells, while 43%, formed by interneurons that were accompanied by glial sibling cells, arose from bipotent NPCs (Figure 5D).

DISCUSSION

We performed detailed lineage tracing of pNPCs from the dorsolateral region of the SVZ. Using the *UbC-StarTrack* clonal methodology, we showed that postnatal SVZ-NPCs gave rise to glial cells that populate the ventricular zone and adjacent areas and interneurons widespread throughout the OB. No glial cells were found in the adult OB after postnatal SVZ electroporation, as previously reported (Figueres-Oñate and López-Mascaraque, 2016). In addition, the presence of clones of olfactory interneurons

and glial cells located within areas adjacent to the SVZ revealed the multipotency of pNPCs. Cell populations arising from targeted pNPCs were highly diverse in terms of clone size and cell dispersion throughout the adult brain. These data reveal the broad coexistence of different SVZ-NPCs *in vivo* at perinatal stages, as well as the presence of bipotential NPCs.

Focusing on the lineage progression of dorsolateral NPCs, previous research has shown that aNPCs can generate TAPs that divide up to three times within the neurogenic niche before differentiating into NBs, giving rise to neuronal lineages (Ponti et al., 2013). We identified sibling cells lining the ventricles that expressed EGFR at 3 days post electroporation (dpe). This indicates that some NPCs divided shortly after electroporation, since NPCs have a cell cycle of 13 h (Capela and Temple, 2002; Zheng et al., 2004).

One of the main features of the adult SVZ neurogenic niche is the long-distance migration of newly generated cells along the RMS to reach their final position in the OB. Our data on cell dispersion throughout the RMS at P20 revealed the organization of sibling NBs on their way to the OB. We established that clonally related NBs migrate in small clusters, and are widespread through the rostrocaudal RMS axis. Previous research has shown that some NBs in the RMS retain their ability to proliferate (Poon et al., 2010; Smith and Luskin, 1998). Upon reaching the OB, NBs begin to radially migrate to their final position where they integrate into the pre-existing neural olfactory circuit (Belluzzi et al., 2003; Carleton et al., 2003), replacing granular and periglomerular cells (Imayoshi et al., 2008). Young neurons reach the GcL and/or GL where they differentiate.

Current clonal analysis reveals that pNPCs are committed to producing OB interneurons that are restricted to either the granular or periglomerular cell layers, with a small proportion of clones located in both. The long-term analyses with *UbC-StarTrack* conducted 6 months after electroporation showed that most cells populating the OB are GCs, as previously reported (Lledo and Saghatelyan, 2005, Figueres-Oñate and López-Mascaraque, 2016). Furthermore, previous data show that dorsal SVZ regions tend to produce superficial GCs, whereas the medial and ventral regions produce mostly PGCs (Merkle et al., 2014), although clone size varies among clonal analyses (Calzolari et al., 2015; Fuentealba et al., 2015).

Our long-term analysis showed a lack of sibling NPCs in the SVZ for 64.29% of the analyzed OB interneuronal clones, likely due to exhaustion of the ventricular NPC pool. This provides supporting evidence for NPC consumption after symmetric divisions to generate TAPs (Obernier et al., 2018). Indeed, the balance between proliferative and quiescent aNPCs is fundamental for the maintenance of the neurogenic niche (Furutachi et al., 2015; Obernier et al., 2018). Proliferative activity decreases to approximately 70% in the aging SVZ, suggesting consumption of the NPC niche (Capilla-Gonzalez et al., 2015).

Previous studies have reported morphological changes in the cytoarchitecture of the aging ventricular niche, with a disruption of the SVZ-RMS axis (Mobley et al., 2013), leaving the main proliferative capability to the dorsolateral ventricular surface (Conover and Shook, 2011). Moreover, there is a reduction in the population of NBs, TAPs (Luo et al., 2006), and NPCs (Ahlenius et al., 2009), along with a deregulation of the NPC cell-cycle machinery by 6 months of age (Daynac et al., 2016). This is in line with previous clonal analyses showing that 58% of the clones produced by aNPCs consist of mature interneurons without NPCs in the ventricular surface (Calzolari et al., 2015).

We also noted the presence of astrocytes and oligodendrocytes arising from pNPCs, as previously described (Tong et al., 2015; Wang et al., 2013). During embryonic development, astrocytes arise from embryonic day 14 (E14) NPCs located in the ventricle. They then migrate along the cortex to their final position where they undergo symmetrical division to increase their population during the first 3 weeks of postnatal development (Ge et al., 2012). Astroglial clones that arise from embryonic NPCs contain up to 50 siblings (García-Marqués and López-Mascaraque, 2013). Here, pNPCs gave rise to smaller astroglial clones, with no more than ten sibling cells. Thus, pNPCs lose their astrogenic proliferative potential compared with embryonic NPCs. In addition to the small number of cells per clone, sibling astrocytes occupied different cortical layers, as described after embryonic NPC targeting (Bribián et al., 2016). Notably, clonal size differed significantly depending on cell lineage. Oligodendrocytes formed larger clones compared with astrocytes or interneurons, and displayed a narrow spatial distribution in contrast to interneurons. In the generation of oligodendroglia, pNPCs undergo an asynchronous maturation. The resulting display of sibling cells with differing degrees of maturation (Zerlin et al., 2004), is correlated with the continuous proliferation of these cells in the adult brain (García-Marqués et al., 2014).

The multipotentiality capability of pNPCs to give rise to neurons, astrocytes, or oligodendrocytes has been reported previously (Ganat et al., 2006; Guo et al., 2009; Ventura and Goldman, 2007). In the adult hippocampus, genetic fate mapping and clonal lineage tracing of NPCs i*n vivo* has shown the generation of neurons and astrocytes, but not oligodendrocytes (Bonaguidi et al., 2011; Encinas et al., 2011). *In vitro* time-lapse analysis has revealed the generation of either neurons or oligodendrocytes from acutely isolated individual precursor cells, but never both

(Ortega et al., 2013). Similarly, *in vivo* clonal analysis has described only neuronal lineages from individual NPCs (Calzolari et al., 2015).

StarTrack is an established clonal analysis methodology employed by several lineage studies to define clones and address the fate potential of cells arising from single NPCs (García-Marqués and López-Mascaraque, 2013, 2017; Martín-López et al., 2013; García-Marqués et al., 2014; Parmigiani et al., 2015; Figueres-Oñate et al., 2015, 2016; Bribian et al., 2018; Cerrato et al., 2018; Redmond et al., 2019; Gutiérrez et al., 2019). Due to ubiquitous promoter expression, *UbC-StarTrack* allows us to conduct precise lineage tracing, regardless of the genes or markers expressed by the cells of interest. In mouse cerebellar WM, the *UbC-StarTrack* methodology has been used to identify bipotent NPCs that produce interneurons and WM astrocytes in embryonic (Parmigiani et al., 2015) and postnatal mice (Cerrato et al., 2018). StarTrack lineage-tracing experiments, targeting embryonic NPCs at E14.5, have reported that postnatal B1 cells and E1 cells originate from a common NPC in the embryonic forebrain (Redmond et al., 2019), and this was also confirmed using *Cre*-driven lineage tracing (Ortiz-Álvarez et al., 2019). These data reveal that ependymal cells and aNPCs share a common embryonic precursor.

Our study is the first *in vivo* clonal analysis showing the bipotency of single pNPCs, including olfactory interneurons and glial cells. The lineage transition between NPCs and their progeny accomplished gradual cell maturation, displaying an overlapping distribution of molecular markers at different time frames in the NPC lineage progression.

This work revealed lineage progression and the clonal relationships between the cell progeny of SVZ pNPCs, including neuronal and glial cells. We uncovered the heterogeneity of cells that exhibited committed and bipotent potentials *in vivo*. Targeted pNPCs produced sibling neurons and glial cells, displaying different clonal patterns in terms of clone size and distribution. Heterogeneity in the cell-fate potential of pNPCs creates additional complexity for neural lineage specification *in vivo*.

EXPERIMENTAL PROCEDURES

Animals

Wild-type C57BL/6 mice from the Cajal Institute animal facility were treated according to the European Union guidelines on the use and welfare of experimental animals (2010/63/EU) as well as those of the Spanish Ministry of Agriculture (RD 1201/2005 and L 32/2007). The CSIC Bioethical Committee and the Community of Madrid approved all the procedures (Ref. PROEX 44/14). The mice gestation period lasted 19 days, considering the day of vaginal plug visualization as E0 and day of birth as P0. In addition, mice from P30 onward were considered adults.

UbC-StarTrack Plasmids

The *UbC-StarTrack* constructs were designed as described previously (Figueres-Oñate et al., 2016). In brief, six different fluorescent proteins were cloned within ubiquitous *PiggyBac* transposable constructs. The selected fluorescent proteins were mT-Sapphire, mCerulean, yellow fluorescent protein (YFP), enhanced green fluorescent protein (EGFP), monomeric Kusabira Orange (mKO), and mCherry. Two *LoxP* sites were included to avoid the expression of non-integrated constructs. Fluorescent proteins were fused to the histone H2B, to be expressed in the cell nucleus. The clonal mixture consists of the addition of the 12 floxed constructs, the hyPBase, and the *Cre*-ERT2 (Figure 1A).

Postnatal Electroporation and Tamoxifen Administration

Pups (P0/P1) were electroporated as described previously (Alvarez-Buylla and Garcia-Verdugo, 2002; Figueres-Oñate and López-Mascaraque, 2016). Tamoxifen (Sigma-Aldrich) was dissolved in pre-warmed corn oil (Sigma-Aldrich) at a final concentration of 20 mg/mL. A single dose of 5 mg/40 g body weight was intraperitoneally administered the day after electroporation. Animals were analyzed at least 2–3 days after tamoxifen injection to allow for inhibition of non-integrated constructs.

Immunohistochemistry

In brief, 50-μm vibratome sections were first permeabilized using 0.5% and 0.1% PBS with Tween 20 (PBS-T), then blocked with 5% normal goat serum for 90 min. Primary antibodies, BLBP (1:300, Abcam ab32423), EGFR (1:200, Millipore 06-847), Sox2 (1:200, Cell Signaling Technology 2748S), Olig2 (1:500, Millipore AB9610), GFAP (1:1,000, Dako 31745), calretinin (1:500, Abcam ab702), or S100β (1:500, Abcam ab41548), were then added to the sections, and sections were incubated overnight at 4°C. Sections were washed in PBS-T and subsequently incubated for 120 min with the secondary antibody conjugated with a far-red fluorophore (1:1,000, Alexa Fluor 633 or 647, Molecular Probes). Finally, after extensive PBS washing, sections were mounted onto glass slides with Mowiol.

Image Acquisition

Fluorescent labeling was checked under an epifluorescence microscope (Nikon Eclipse E600) with the appropriate filter cubes (Semrock): UV-2A (FF01-334/40-25) Cerulean (FF01-405/10), GFP (FF01-473/10), YFP (FF01-520/15), mKO (FF01-540/15), mCherry (FF01-590/20), and Cy5 (FF02-628/40-25). Images were acquired on a Leica TCS-SP5 confocal microscope, capturing the different fluorescent proteins (XFPs) in separate channels. The wavelength of excitation (Ex) and emission (Em) for each XFP were (in nanometers): mT-Sapphire (Ex: 405; Em: 520–535), mCerulean (Ex: 458; Em: 468–480), EGFP (Ex: 488; Em: 498–510), YFP (Ex: 514; Em: 525–535), mKO (Ex: 514; Em: 560–580), mCherry (Ex: 561; Em: 601–620), and Alexa Fluor 633/647 (Ex: 633; Em: 650–760). Confocal laser lines were between 25% and 40% in all cases. Maximum projection images were created using LASAF Leica and NIH-ImageJ software.

Clonal Analysis

Confocal images were analyzed with a custom-designed macro integrated into ImageJ software (NIH). First, background subtraction from each image was done using a smooth filter to improve cell signal selection. A specific threshold was then applied for each fluorophore. Once cell selections were determined, a binary image was created comprising the labeled cells in all the channels. A watershed filter was applied to the binary image to isolate contiguous tagged cells and analyze them as individual points. Thereafter, the minimal range of fluorescence intensity to be considered as positive fluorescent labeling was determined. Thus, a color code was assigned for each labeled cell including intensity values for each fluorophore. Further analysis was performed to determine sibling cells ontogeny based on the location of the fluorophore (nucleus or cytoplasm). All data were processed using Leica Application Suite Advanced Fluorescence (LAS AF) to generate the images, and later on using an NIH-ImageJ self-developed macro. Clone dispersion reconstructions were achieved with the advantage of the Reconstruct software (SynapseWeb).

Statistics

Statistical parameters were determined using SigmaPlot (Systat) or Prism (GraphPad) software. Statistical significance between groups was addressed either by two-tailed unpaired Student's t tests or one-way analysis of variance. A confidence interval of 95% ($p < 0.05$) was required to consider values statistically significant. Throughout the study, values were represented as the mean ± SEM. Statistically significant differences across the groups are indicated in illustrations by asterisks: *$p < 0.05$, **$p < 0.01$, ***$p < 0.001$. Outliers were excluded from the analysis, as they were considered extreme values that deviate from other observations (oligodendroglial clone 561 cells and two interneuronal clones of 52 and 58 cells, respectively). Graphs were obtained either from Microsoft Excel software, Prism 6 (GraphPad), or the online plug-in plotly (https://plot.ly/).

SUPPLEMENTAL INFORMATION

Supplemental Information can be found online at https://doi.org/10.1016/j.stemcr.2019.08.010.

AUTHOR CONTRIBUTIONS

M.F.-O. conceived and designed the study, performed experiments, analyzed the data, and wrote the manuscript. M.S.-V. and R.S.-G. participated in tissue processing, confocal microscopy, and clonal analyses. L.L-M conceived and designed the study and wrote the manuscript. All authors discussed the results and contributed to the final manuscript.

ACKNOWLEDGMENTS

We are thankful to the Animal Facility staff for their assistance. We are also very grateful to Carmen Hernandez and Belen Garcia from the Imaging and Microscopy Facility for their support with ImageJ macro design and confocal microscopy, along with Emilio Tejera for his technical assistance. The authors also thank Hayley Colman, Michael Kawaja, and Rebekah Jordan Barnett for their English review of the manuscript. This work was supported by research grant number BFU2016-75207-R from the Spanish Ministry of Economy and Competitiveness.

Received: March 3, 2019
Revised: August 21, 2019
Accepted: August 21, 2019
Published: September 19, 2019

REFERENCES

Ahlenius, H., Visan, V., Kokaia, M., Lindvall, O., and Kokaia, Z. (2009). Neural stem and progenitor cells retain their potential for proliferation and differentiation into functional neurons despite lower number in aged brain. J. Neurosci. *29*, 4408–4419.

Alvarez-Buylla, A., and Garcia-Verdugo, J.M. (2002). Neurogenesis in adult subventricular zone. J.Neurosci. *22*, 629–634.

Beckervordersandforth, R., Tripathi, P., Ninkovic, J., Bayam, E., Lepier, A., Stempfhuber, B., Kirchhoff, F., Hirrlinger, J., Haslinger, A., Lie, D.C., et al. (2010). In vivo fate mapping and expression analysis reveals molecular hallmarks of prospectively isolated adult neural stem cells. Cell Stem Cell *7*, 744–758.

Belluzzi, O., Benedusi, M., Ackman, J., and LoTurco, J.J. (2003). Electrophysiological differentiation of new neurons in the olfactory bulb. J. Neurosci. *23*, 10411–10418.

Bonaguidi, M.A., Wheeler, M.A., Shapiro, J.S., Stadel, R.P., Sun, G.J., Ming, G.L., and Song, H. (2011). In vivo clonal analysis reveals self-renewing and multipotent adult neural stem cell characteristics. Cell. *145*, 1142–1155.

Bribián, A., Figueres-Oñate, M., Martín-López, E., and López-Mascaraque, L. (2016). Decoding astrocyte heterogeneity: new tools for clonal analysis. Neuroscience *323*, 10–19.

Bribian, A., Pérez-Cerdá, F., Matute, C., and López-Mascaraque, L. (2018). Clonal glial response in a multiple sclerosis mouse model. Front. Cell. Neurosci. *23*, 375.

Calzolari, F., Michel, J., Baumgart, E.V., Theis, F., Götz, M., and Ninkovic, J. (2015). Fast clonal expansion and limited neural stem cell self-renewal in the adult subependymal zone. Nat. Neurosci. *18*, 490–492.

Capela, A., and Temple, S. (2002). LeX/ssea-1 is expressed by adult mouse CNS stem cells identifying them as nonependymal. Neuron *35*, 865–875.

Capilla-Gonzalez, V., Herranz-Pérez, V., and García-Verdugo, J.M. (2015). The aged brain: genesis and fate of residual progenitor cells in the subventricular zone. Front. Cell. Neurosci. *9*, 365.

Carleton, A., Petrenanu, L., Lansford, R., Alvarez-Buylla, A., and Lledo, P.-M. (2003). Becoming a new neuron in the adult OB. Nat. Neurosci. *6*, 507–518.

Cerrato, V., Parmigiani, E., Betizeau, M., Aprato, J., Nanavaty, I., Berchialla, P., Luzzati, F., de'Sperati, C., López-Mascaraque, L., and Buffo, A. (2018). Multiple origins and modularity in the spatiotemporal emergence of cerebellar astrocyte heterogeneity. PLoS Biol. *16*, e2005513.

Codega, P., Silva-Vargas, V., Paul, A., Maldonado-Soto, A.R., Deleo, A.M., Pastrana, E., and Doetsch, F. (2014). Prospective

identification and purification of quiescent adult neural stem cells from their in vivo niche. Neuron *82*, 545–559.

Conover, J.C., and Shook, B.A. (2011). Aging of the subventricular zone neural stem cell niche. Aging Dis. *2*, 49–63.

Daynac, M., Morizur, L., Chicheportiche, A., Mouthon, M.A., and Boussin, F.D. (2016). Age-related neurogenesis decline in the subventricular zone is associated with specific cell cycle regulation changes in activated neural stem cells. Sci. Rep. *6*, 1–10.

Dimou, L., and Götz, M. (2014). Glial cells as progenitors and stem cells: new roles in the healthy and diseased brain. Physiol. Rev. *94*, 709–737.

Doetsch, F., and Alvarez-Buylla, A. (1996). Network of tangential pathways for neuronal migration in adult mammalian brain. Proc. Natl. Acad. Sci. U S A *93*, 14895–14900.

Encinas, J.M., Michurina, T.V., Peunova, N., Park, J.H., Tordo, J., Peterson, D.A., Fishell, G., Koulakov, A., and Enikolopov, G. (2011). Division-coupled astrocytic differentiation and age-related depletion of neural stem cells in the adult hippocampus. Cell Stem Cell *8*, 566–579.

Figueres-Oñate, M., García-Marqués, J., and López-Mascaraque, L. (2016). UbC-StarTrack a clonal method to target the entire progeny of individual progenitors. Sci. Rep. *2016*, 33896.

Figueres-Oñate, M., García-Marqués, J., Pedraza, M., De Carlos, J.A., and López-Mascaraque, L. (2015). Spatiotemporal analyses of neural lineages after embryonic and postnatal progenitor targeting combining different reporters. Front. Neurosci. *9*, 1–11.

Figueres-Oñate, M., and López-Mascaraque, L. (2016). Adult olfactory bulb interneuron phenotypes identified by targeting embryonic and postnatal neural progenitors. Front. Neurosci. *10*, 1–12.

Fiorelli, R., Azim, K., Fischer, B., and Raineteau, O. (2015). Adding a spatial dimension to postnatal ventricular-subventricular zone neurogenesis. Development *142*, 2109–2120.

Fuentealba, L.C., Rompani, S.B., Parraguez, J.I., Obernier, K., Romero, R., Cepko, C.L., and Alvarez-Buylla, A. (2015). Embryonic origin of postnatal neural stem cells. Cell *161*, 1644–1655.

Furutachi, S., Miya, H., Watanabe, T., Kawai, H., Yamasaki, N., Harada, Y., Imayoshi, I., Nelson, M., Nakayama, K.I., Hirabayashi, Y., and Gotoh, Y. (2015). Slowly dividing neural progenitors are an embryonic origin of adult neural stem cells. Nat. Neurosci. *18*, 657–665.

Ganat, Y.M., Silbereis, J., Cave, C., Ngu, H., Anderson, G.M., Ohkubo, Y., Ment, L.R., and Vaccarino, F.M. (2006). Early postnatal astroglial cells produce multilineage precursors and neural stem cells in vivo. J. Neurosci. *26*, 8609–8621.

García-Marqués, J., and López-Mascaraque, L. (2013). Clonal identity determines astrocyte cortical heterogeneity. Cereb. Cortex *23*, 1463–1472.

García-Marqués, J., and López-Mascaraque, L. (2017). Clonal mapping of astrocytes in the olfactory bulb and rostral migratory stream. Cereb. Cortex *27*, 2195–2209.

García-Marqués, J., Núñez-Llaves, R., and López-Mascaraque, L. (2014). NG2-glia from pallial progenitors produce the largest clonal clusters of the brain: time frame of clonal generation in cortex and olfactory bulb. J. Neurosci. *34*, 2305–2313.

Ge, W.P., Miyawaki, A., Gage, F.H., Jan, Y.N., and Jan, L.Y. (2012). Local generation of glia is a major astrocyte source in postnatal cortex. Nature *484*, 376–380.

Guo, F., Ma, J., McCauley, E., Bannerman, P., and Pleasure, D. (2009). Early postnatal proteolipid promoter-expressing progenitors produce multilineage cells in vivo. J. Neurosci. *29*, 7256–7270.

Gutiérrez, Y., García-Marqués, J., Liu, X., Fortes-Marco, L., Sánchez-González, R., Giaume, C., and López-Mascaraque, L. (2019). Sibling astrocytes share preferential coupling via gap junctions. Glia *67*, 1–7.

Ihrie, R.A., Shah, J.K., Harwell, C.C., Levine, J.H., Guinto, C.D., Lezameta, M., Kriegstein, A.R., and Alvarez-Buylla, A. (2011). Persistent sonic hedgehog signaling in adult brain determines neural stem cell positional identity. Neuron *71*, 250–262.

Imayoshi, I., Sakamoto, M., Ohtsuka, T., Takao, K., Miyakawa, T., Yamaguchi, M., Mori, K., Ikeda, T., Itohara, S., and Kageyama, R. (2008). Roles of continuous neurogenesis in the structural and functional integrity of the adult forebrain. Nat. Neurosci. *11*, 1153–1161.

Kriegstein, A., and Alvarez-Buylla, A. (2009). The glial nature of embryonic and adult neural stem cells. Ann. Rev. Neurosci. *32*, 149–184.

Laywell, E.D., Rakic, P., Kukekov, V.G., Holland, E.C., and Steindler, D.A. (2000). Identification of a multipotent astrocytic stem cell in the immature and adult mouse brain. Proc. Natl. Acad. Sci. U S A *97*, 13883–21388.

Levison, S.W., and Goldman, J.E. (1997). Multipotential and lineage restricted precursors coexist in the mammalian perinatal subventricular zone. J.Neurosci. Res. *48*, 83–94.

Lledo, P.M., and Saghatelyan, A. (2005). Integrating new neurons into the adult olfactory bulb: joining the network life-death decisions and the effects of sensory experience. Trends Neurosci. *28*, 248–254.

Llorens-Bobadilla, E., Zhao, S., Baser, A., Saiz-Castro, G., Zwadlo, K., and Martin-Villalba, A. (2015). Single-cell transcriptomics reveals a population of dormant neural stem cells that become activated upon brain injury. Cell Stem Cell *17*, 329–340.

Luo, J., Daniels, S.B., Lennington, J.B., Notti, R.Q., and Conover, J.C. (2006). The aging neurogenic subventricular zone. Aging Cell *5*, 139–152.

Ma, J., Shen, Z., Yu, Y.C., and Shi, S.H. (2018). Neural lineage tracing in the mammalian brain. Curr. Opin. Neurobiol. *50*, 7–16.

Martín-López, E., García-Marques, J., Núñez-Llaves, R., and López-Mascaraque, L. (2013). Clonal astrocytic response to cortical injury. PLoS One *8*, e74039.

Merkle, F.T., Fuentealba, L.C., Sanders, T.A., Magno, L., Kessaris, N., and Alvarez-Buylla, A. (2014). Adult neural stem cells in distinct microdomains generate previously unknown interneuron types. Nat. Neurosci. *17*, 207–214.

Merkle, F.T., Tramontin, A.D., García-Verdugo, J.M., and Alvarez-Buylla, A. (2004). Radial glia give rise to adult neural stem cells in the subventricular zone. Proc. Natl. Acad. Sci. U S A *101*, 17528–17532.

Mobley, A.S., Bryant, A.K., Richard, M.B., Brann, J.H., Firestein, S.J., and Greer, C.A. (2013). Age-dependent regional changes in the rostral migratory stream. Neurobiol. Aging *34*, 1873–1881.

Obernier, K., Cebrian-Silla, A., Thomson, M., Parraguez, J.I., Anderson, R., Guinto, C., Rodas Rodriguez, J., Garcia-Verdugo, J.M., and Alvarez-Buylla, A. (2018). Adult neurogenesis is sustained by symmetric self-renewal and differentiation. Cell Stem Cell *22*, 221–234.

Obernier, K., and Alvarez-Buylla, A. (2019). Neural stem cells: origin heterogeneity and regulation in the adult mammalian brain. Development *146*, 1–15.

Ortega, F., Gascón, S., Masserdotti, G., Deshpande, A., Simon, C., Fischer, J., Dimou, L., Chichung Lie, D., Schroeder, T., and Berninger, B. (2013). Oligodendrogliogenic and neurogenic adult subependymal zone neural stem cells constitute distinct lineages and exhibit differential responsiveness to Wnt signalling. Nat. Cell Biol. *15*, 602–613.

Ortiz-Álvarez, G., Daclin, M., Shihavuddin, A., Lansade, P., Fortoul, A., Faucourt, M., Clavreul, S., Lalioti, M.E., Taraviras, S., Hippenmeyer, S., et al. (2019). Adult neural stem cells and multiciliated ependymal cells share a common lineage regulated by the geminin family members. Neuron *102*, 159–172.

Parmigiani, E., Leto, K., Rolando, C., Figueres-Oñate, M., López-Mascaraque, L., Buffo, A., and Rossi, F. (2015). Heterogeneity and bipotency of astroglial-like cerebellar progenitors along the interneuron and glial lineages. J. Neurosci. *35*, 7388–7402.

Ponti, G., Obernier, K., Guinto, C., Jose, L., Bonfanti, L., and Alvarez-Buylla, A. (2013). Cell cycle and lineage progression of neural progenitors in the ventricular-subventricular zones of adult mice. Proc. Natl. Acad. Sci. U S A *110*, E1045–E1054.

Poon, A., Li, Z., Wolfe, G.W., Lu, L., Williams, R.W., Hayes, N.L., Nowakowski, R.S., and Goldowitz, D. (2010). Identification of a Chr 11 quantitative trait locus that modulates proliferation in the rostral migratory stream of the adult mouse brain. Europ. J. Neurosci. *32*, 523–537.

Redmond, S.A., Figueres-Oñate, M., Obernier, K., Nascimento, M.A., Parraguez, J.I., López-Mascaraque, L., Fuentealba, L.C., and Alvarez-Buylla, A. (2019). Development of ependymal and postnatal neural stem cells and their origin from a common embryonic progenitor. Cell Rep. *27*, 429–441.

Smith, C.M., and Luskin, M.B. (1998). Cell cycle length of olfactory bulb neuronal progenitors in the rostral migratory stream. Dev. Dyn. *213*, 220–227.

Tong, C.K., Fuentealba, L.C., Shah, J.K., Lindquist, R.A., Ihrie, R.A., Guinto, C.D., Rodas-Rodriguez, J.L., and Alvarez-Buylla, A. (2015). A dorsal SHH-dependent domain in the V-SVZ produces large numbers of oligodendroglial lineage cells in the postnatal brain. Stem Cell Reports *5*, 461–470.

Ventura, R.E., and Goldman, J.E. (2007). Dorsal radial glia generate olfactory bulb interneurons in the postnatal murine brain. J. Neurosci. *16*, 4297–4302.

Wang, X., Chang, L., Guo, Z., Li, W., Liu, W., Cai, B., and Wang, J. (2013). Neonatal SVZ EGFP-labeled cells produce neurons in the olfactory bulb and astrocytes in the cerebral cortex by in-vivo electroporation. Neuroreport *24*, 381–387.

Willaime-Morawek, S., Seaberg, R.M., Batista, C., Labbé, E., Attisano, L., Gorski, J.A., Jones, K.R., Kam, A., Morshead, C.M., and van der Kooy, D. (2006). Embryonic cortical neural stem cells migrate ventrally and persist as postnatal striatal stem cells. J. Cell Biol. *175*, 159–168.

Young, K.M., Fogarty, M., Kessaris, N., and Richardson, W.D. (2007). Subventricular zone stem cells are heterogeneous with respect to their embryonic origins and neurogenic fates in the adult olfactory bulb. J. Neurosci. *27*, 8286–8296.

Zerlin, M., Milosevic, A., and Goldman, J.E. (2004). Glial progenitors of the neonatal subventricular zone differentiate asynchronously leading to spatial dispersion of glial clones and to the persistence of immature glia in the adult mammalian CNS. Dev. Biol. *270*, 200–213.

Zheng, W., Nowakowski, S., and Vaccarino, F.M. (2004). Fibroblast growth factor 2 is required for maintaining the neural stem cell pool in the mouse brain subventricular zone. Dev. Neurosci. *26*, 181–196.

Stem Cell Reports, Volume *13*

Supplemental Information

Lineage Tracing and Cell Potential of Postnatal Single Progenitor Cells *In Vivo*

María Figueres-Oñate, Mario Sánchez-Villalón, Rebeca Sánchez-González, and Laura López-Mascaraque

Table S1

Figueres-Oñate et al., 2016

1	2	3	4	5	6	N=1	N=2	N=3	N=4	N=5	fa	f %	Original Positon
0	0	0	0	0	0	0	0	0	0	0	0	0,00	1
0	2	3	0	0	6	0	1	0	0	0	1	0,01	2
0	0	3	4	0	6	2	0	0	1	0	3	0,04	3
1	2	3	0	0	6	0	1	1	2	0	4	0,06	4
1	0	3	4	0	0	1	1	1	1	2	6	0,09	5
0	2	0	0	0	6	2	0	3	2	0	7	0,10	6
0	2	3	4	0	6	2	3	1	0	3	9	0,13	7
0	2	3	0	5	0	0	9	2	0	0	11	0,16	8
1	0	0	4	5	0	0	0	9	0	2	11	0,16	9
1	0	3	4	0	6	0	1	0	2	8	11	0,16	10
1	0	3	4	5	0	4	1	5	1	1	12	0,18	11
0	2	3	0	0	0	1	12	1	0	0	14	0,21	12
0	2	3	0	5	6	3	10	5	1	0	19	0,28	13
1	2	0	0	5	0	6	3	7	0	3	19	0,28	14
0	2	0	0	5	0	2	7	11	0	0	20	0,30	15
1	2	3	0	5	0	7	3	3	0	8	21	0,31	16
1	0	3	0	0	0	1	9	4	0	8	22	0,33	17
1	0	0	4	0	6	1	0	2	1	20	24	0,36	18
1	2	3	0	0	0	0	0	15	0	9	24	0,36	19
1	0	3	0	0	6	0	14	0	0	13	27	0,40	20
1	2	3	4	5	0	4	4	9	1	9	27	0,40	21
1	2	3	4	0	6	6	0	0	5	17	28	0,42	22
1	2	0	4	5	0	8	7	15	0	1	31	0,46	23
1	2	3	4	0	0	3	5	15	0	11	34	0,51	24
0	0	3	0	0	6	5	27	3	1	2	38	0,57	25
0	2	0	4	5	0	6	15	13	2	5	41	0,61	26
1	2	0	0	0	6	8	1	0	22	10	41	0,61	27
1	0	0	0	5	0	3	8	31	0	1	43	0,64	28
0	2	0	4	0	6	3	22	1	8	10	44	0,66	29
1	0	0	4	0	0	3	2	22	4	14	45	0,67	30
1	0	0	4	5	6	7	3	11	1	23	45	0,67	31
0	2	0	0	5	6	6	5	23	12	0	46	0,69	32
0	2	3	4	0	0	4	35	6	1	1	47	0,70	33
1	2	0	0	0	0	20	2	13	0	13	48	0,72	34
1	2	0	0	5	6	15	2	6	20	5	48	0,72	35
0	2	3	4	5	0	6	28	3	1	11	49	0,73	36
0	2	0	4	5	6	30	7	13	2	3	55	0,82	37
1	2	0	4	0	0	7	2	27	8	17	61	0,91	38
1	2	3	0	5	6	19	25	5	7	6	62	0,93	39
0	0	3	4	5	0	13	17	20	0	13	63	0,94	40
1	2	0	4	0	6	10	0	2	24	28	64	0,96	41
0	0	0	4	0	6	9	9	5	10	32	65	0,97	42
0	0	3	4	0	0	14	30	17	1	3	65	0,97	43
0	2	3	4	5	6	19	31	8	0	7	65	0,97	44
1	0	0	0	0	0	1	38	7	16	10	72	1,08	45
1	2	0	4	5	6	27	2	11	19	20	79	1,18	46
1	0	3	0	5	0	2	44	26	0	8	80	1,20	47
0	2	0	0	0	0	4	38	37	2	0	81	1,21	48
0	0	3	4	5	6	32	40	19	1	8	100	1,49	49
1	0	3	4	5	6	15	42	22	0	21	100	1,49	50
0	0	0	4	5	0	34	18	50	3	4	109	1,63	**51**
1	0	0	0	0	6	3	3	0	32	117	155	2,32	**52**
1	0	0	0	5	6	25	51	40	22	21	159	2,38	**53**
0	0	0	0	0	6	7	21	18	90	39	175	2,62	**54**
0	0	0	4	5	6	64	21	54	39	18	196	2,93	**55**
1	2	3	4	5	6	66	21	39	17	57	200	2,99	**56**
0	0	3	0	5	6	110	112	83	24	2	331	4,95	**57**
0	2	0	4	0	0	43	143	84	62	28	360	5,38	**58**
0	0	3	0	5	0	50	174	127	9	13	373	5,58	**59**
1	0	3	0	5	6	59	179	101	4	37	380	5,68	**60**
0	0	3	0	0	0	16	312	82	5	26	441	6,59	**61**
0	0	0	4	0	0	102	119	155	66	32	474	7,09	**62**
0	0	0	0	5	0	74	136	375	48	35	668	9,99	**63**
0	0	0	0	5	6	271	125	225	108	8	737	11,02	**64**
						1265	**2001**	**1893**	**708**	**823**	**6690**	**100,00**	

Frequent combinations

Figueres-Oñate et al., 2019

1	2	3	4	5	6	fa	f %	Original Positon	VALUE	Actuall Positon
0	0	0	0	0	0	7	0,01	1	=	1
0	2	3	0	0	6	9614	0,05	2	=	2
0	2	3	0	5	0	4147	0,06	8	↗	3
0	2	3	0	5	6	5357	0,09	13	↗	4
1	0	3	4	5	0	7219	0,11	11	↗	5
0	2	0	0	0	6	944	0,11	6	=	6
0	2	0	0	5	0	1155	0,12	15	↗	7
0	2	3	0	0	0	1395	0,15	12	↗	8
0	2	0	0	5	6	9085	0,15	32	↗	9
1	0	0	4	5	0	1816	0,19	9	↘	10
1	0	3	4	0	0	2163	0,21	5	↘	11
1	2	3	0	5	0	2364	0,22	16	↗	12
1	2	0	0	5	0	1235	0,25	14	↗	13
1	2	0	4	5	0	658	0,25	23	↗	14
0	2	0	0	0	0	535	0,28	48	↗	15
1	2	3	4	5	0	1323	0,28	21	↗	16
0	2	3	4	0	6	280	0,35	7	↘	17
0	2	0	4	5	0	112	0,37	26	↗	18
0	2	0	4	0	6	118	0,42	29	↗	19
0	2	0	4	5	6	157	0,46	37	↗	20
1	0	3	4	0	6	2353	0,49	10	↘	21
0	2	3	4	5	0	424	0,50	36	↗	22
1	0	3	0	5	0	380	0,52	47	↗	23
0	0	3	4	5	0	465	0,53	40	↗	24
1	0	0	4	0	6	156	0,55	18	↘	25
1	0	0	4	5	6	51	0,61	31	↗	26
0	0	3	4	0	6	56	0,65	3	↘	27
0	2	3	4	5	6	89	0,68	44	↗	28
1	2	0	4	0	6	974	0,77	41	↗	29
1	0	3	4	5	6	359	0,81	50	↗	30
1	2	3	4	0	0	513	0,82	24	↘	31
0	0	0	4	0	6	688	0,93	42	↗	32
1	0	0	4	0	0	6727	0,95	30	↘	33
0	2	3	4	0	0	3755	0,96	33	↘	34
1	2	3	0	0	0	1163	0,96	19	↘	35
1	2	0	4	5	6	2303	1,07	46	↗	36
0	0	0	4	5	0	965	1,14	**51**	↗	37
1	0	0	0	5	0	557	1,14	28	↘	38
1	2	0	4	0	0	195	1,19	38	↘	39
0	0	3	4	0	0	621	1,21	43	↗	40
1	2	3	0	5	6	1746	1,24	39	↘	41
1	2	3	0	0	6	1366	1,27	4	↘	42
0	0	3	4	5	6	529	1,30	49	↗	43
1	0	3	0	0	6	1836	1,34	20	↘	44
0	0	0	4	5	6	217	1,37	**55**	↗	45
1	2	0	0	5	6	497	1,40	35	↘	46
1	2	0	0	0	6	111	1,63	27	↘	47
1	0	3	0	0	0	821	1,72	17	↘	48
0	0	3	0	0	6	2121	1,79	25	↘	49
1	0	3	0	5	6	1657	1,81	**60**	↗	50
1	2	0	0	0	0	253	2,09	34	↘	51
0	0	3	0	5	0	1426	2,13	**59**	↗	52
1	0	0	0	5	6	1211	2,26	**53**	=	53
0	2	0	4	0	0	779	2,31	**58**	↗	54
0	0	3	0	5	6	255	2,32	**57**	↗	55
1	2	3	4	0	6	1086	2,37	22	↘	56
1	0	0	0	0	6	976	3,69	**52**	↘	57
0	0	0	0	5	0	1291	4,08	**63**	↗	58
0	0	0	0	5	6	222	5,27	**64**	↗	59
1	2	3	4	5	6	1261	5,92	**56**	↘	60
1	0	0	0	0	0	837	6,61	45	↘	61
0	0	0	4	0	0	2413	7,10	**62**	=	62
0	0	3	0	0	0	283	8,93	**61**	↘	63
0	0	0	0	0	6	6024	9,45	**54**	↘	64
						101696	**100,00**			

Frequent combinations

Table S1. Frequency of the fluorescent combinations using the UbC-StarTrack clonal method.

Figure S1

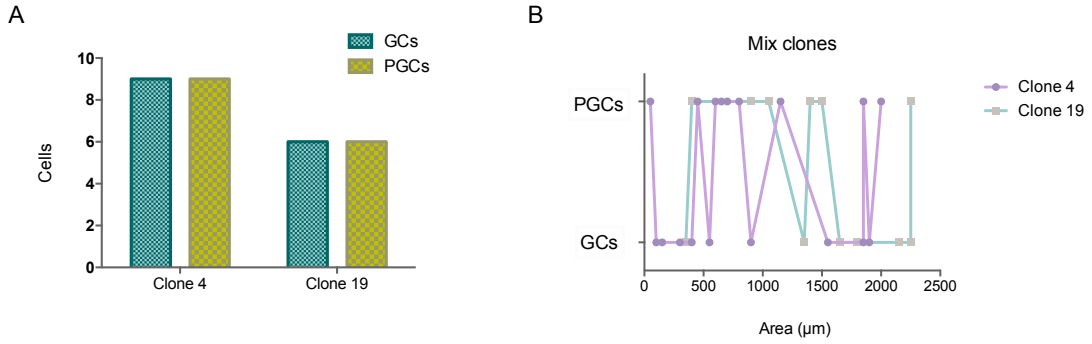

Figure S1.

A. The proportion of sibling GCs and PGCs within mix clones was equitable in both examples presented within our clonal analysis.
B. Sibling GCs and PGCs presented a random dispersion along the rostro-caudal axis in both mix clones (Clone 4 and Clone 19).

Figure S2

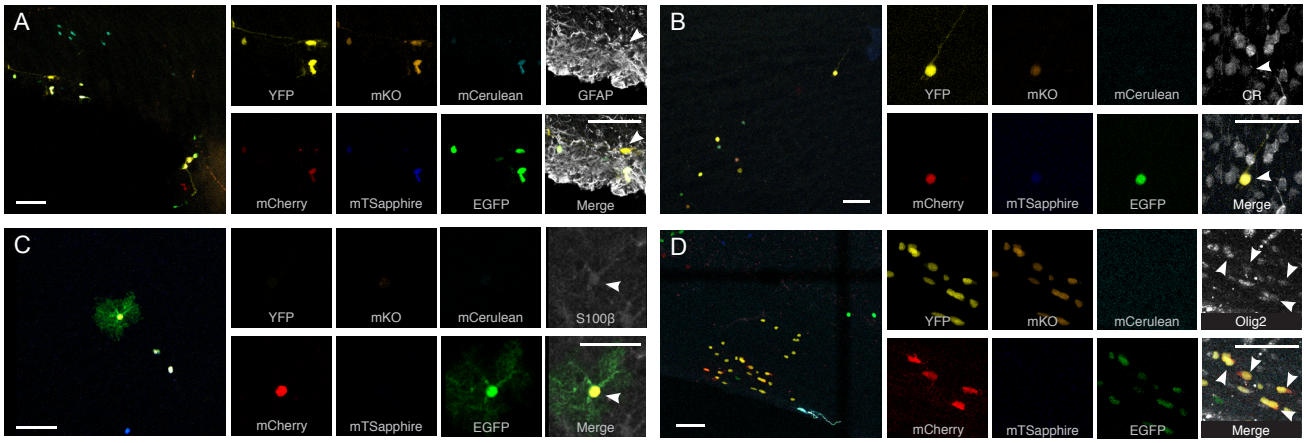

Figure S2.

A. GFAP staining can be used to label NPCs in the SVZ close to the lateral ventricle. The six fluorescent reporter proteins are included into different channels showing the color code of GFAP positive single NPC.
B. UbC-StarTrack labeled interneurons co-expressed Calretinin antibody.
C. To identify the astroglial population, S100β immunostaining was performed. Labeled protoplasmic astrocytes with UbC-StarTrack colocalized with the antibody.
D. Cells from the oligodendroglial lineage were identified using Olig2 immunomarker.
Arrowheads display the sibling cells that co-expressed with the antibodies.
Scale bars 50 μm.

Figure S3

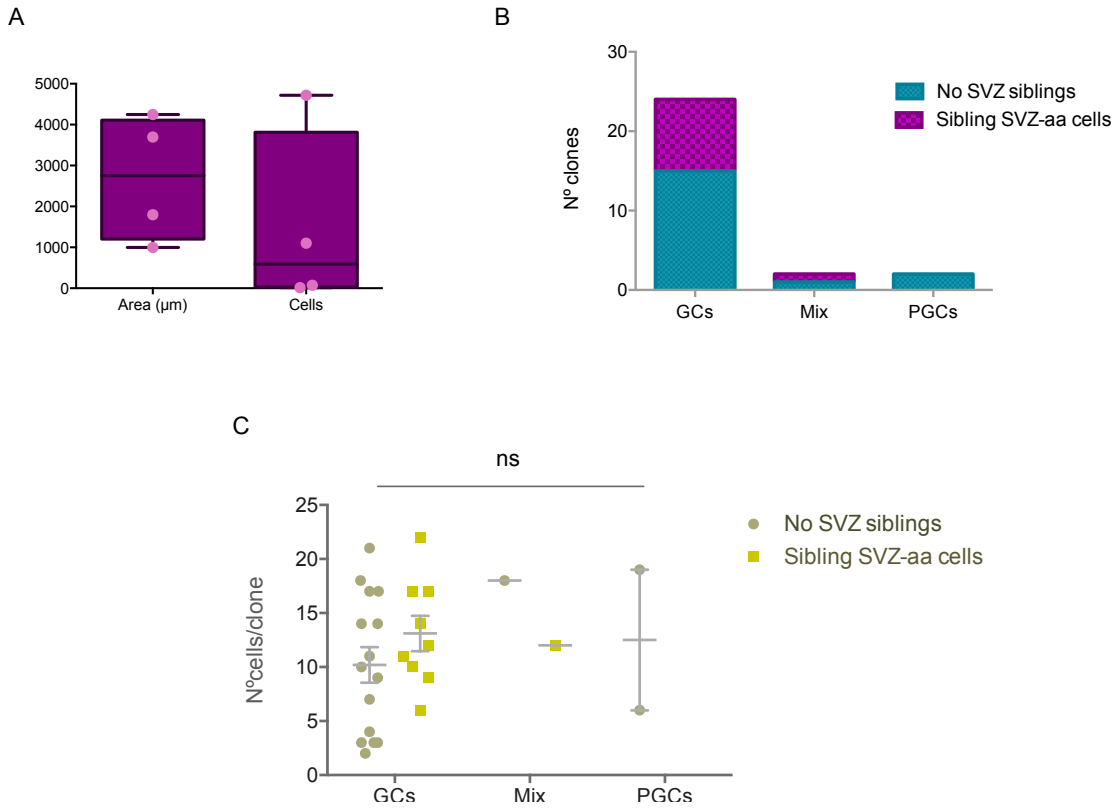

Figure S3

A. An average of 1477 ± 1109 labeled cells were present in the telencephalic region of four different analyzed animals. The average of cortical areas containing sparsed cells was 2688 ± 769 µm. Box plots show all values, from minimal to maximal among the median bar.
B. The proportion of clones that presented sibling cells in the SVZ-aa is maintained within distinct interneuronal clonal types.
C. Clone size was not significant different between clones of interneurons with the different layer-conformation.
Statistical significance across the groups is indicated as follows: ns, nonsignificant, $P > 0.05$; *, $P \leq 0.05$; **, $P \leq 0.01$; ***, $P \leq 0.001$.

Figure S4

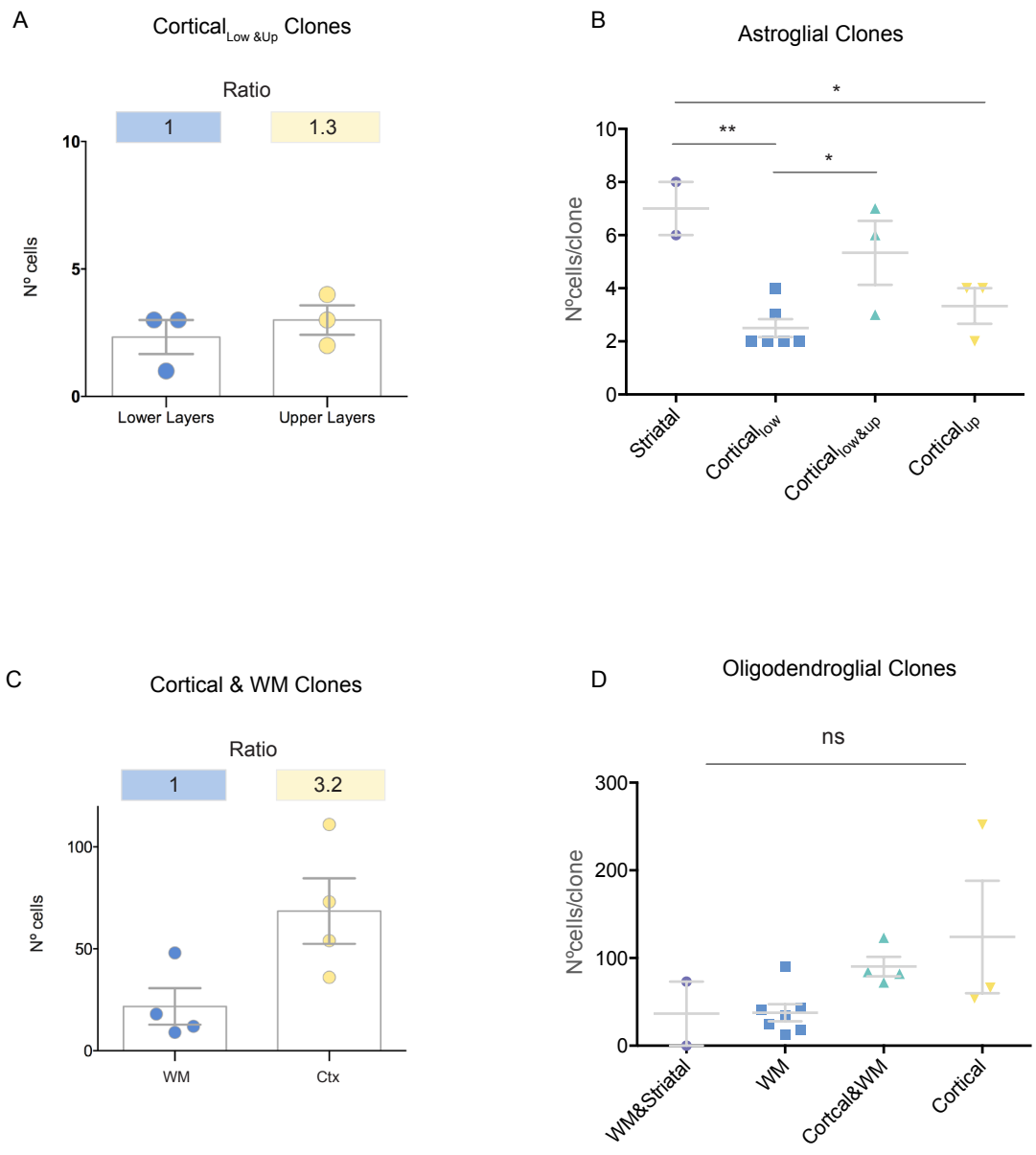

Figure S4

A. Cortical$_{low\&up}$ clones of astrocytes presented sibling astrocytes located in lower/upper layers in a 1 : 1.3 ratio.
B. Variation of the astrocyte clone size related to the distribution through ventricular adjacent areas. Striatal clones displayed the highest number of siblings (7 ± 1 cells/clone). No significant differences were found within Cortical$_{up}$ clones (3.33 ± 0.66 cells/clone) and Cortical$_{low\&up}$ clones (5.33 ± 1.2) or Cortical$_{low}$ clones (2.5 ± 0.34 cells/clone).
C. In oligodendroglial Cortical&WM clones sparsed within the subcortical white matter and the cortex, cells were preferentially positioned in the cortical layer in a 1 : 3.2 ratio.
D. Regarding to clone size, there were no significant differences in the distinct oligodendroglial clones types regarding their siblings distribution through the SVZ adjacent areas.
Statistical significance across the groups is indicated as follows: ns, nonsignificant, $P > 0.05$; *, $P \leq 0.05$; **, $P \leq 0.01$; ***, $P \leq 0.001$.